Journal of Power Sources 235 (2013) 226–233

Contents lists available at SciVerse ScienceDirect

Journal of Power Sources

journal homepage: www.elsevier.com/locate/jpowsour

Nano-structured gas diffusion electrode – A high power and stable cathode material for rechargeable Li-air batteries

H. Cheng*, K. Scott

School of Chemical Engineering & Advanced Materials, Newcastle University, NE1 7RU, United Kingdom

HIGHLIGHTS

- Nano-structured GDE is fabricated and used in a rechargeable Li-air battery.
- The battery has high capacity, long cycle lifetime and good rate capability.
- Improvement mechanism is proposed from electrochemical and spectroscopic evidences.

ARTICLE INFO

Article history:
Received 17 October 2012
Received in revised form
29 January 2013
Accepted 6 February 2013
Available online 19 February 2013

Keywords:
Rechargeable Li–air batteries
Gas diffusion electrode
Air cathode
Nano-structured material
Energy storage

ABSTRACT

The rechargeable Li-air battery has a key role to play for future renewable energy and electric vehicle industries due to its high energy density. However, it suffers from cycling fading and low rate capability, mainly caused by the problem of cathode. Here we create a nanoporous three-dimensional gas diffusion electrode to replace a conventional composite electrode, prolonging battery cycle life over 200 cycles with higher rate capabilities and high capacities. Electrochemical and spectroscopic characterisations indicate the mechanism for the improvement.

1. Introduction

Clean energy supplies are required to combat the unprecedented threat from climate change and environmental pollution. Renewable energy has been considered as a major energy source of tomorrow but its generation is fluctuating. Batteries could serve as a buffer to introduce more renewable energy into the electricity supply grid. Current transportation section heavily depends on the supply of fossil fuels, which contributes significantly to environmental pollution and climate change. Electric cars appear as a realistic alternative for combustion engine cars. Unfortunately, current Li-ion batteries are not yet suited for use in sustainable electrified road transport because they are expensive and can store only a limited amount of energy (up to around 160 km) between charges, causing driver's range anxiety that the battery will peter out while driving [1,2]. One promising alternative to Li-ion batteries for renewable energy and electric car applications is the rechargeable Li-air battery, largely due to its high energy density, which is nearly ten times greater than Li-ion batteries and is comparable to that of petrol and diesel. In addition, it is environmentally friendly (owing to using the oxygen from the air to replace expensive chemicals) and could be light, compact and cost-effective [3–7]. However, it requires significant improvement in stability and rate capability for commercial applications [3–7]. There is a three phase region in the cathode involving gas reactant (oxygen), liquid electrolyte and solid electrode materials within the Li-air battery, which greatly affects the battery capacity and durability [8,9]. Such a unique feature means that the cathode structure plays a critical role and there is a great opportunity for nano-structured material applications. Currently, composite electrodes (CE), fabricated by a casting technique, have been widely used [3–8,10,11]. During the casting process, powders of catalyst, carbon and binder were cast into electrode films with dense structure that has great diffusion resistance for electrochemical active species, leading to significant degradation even at small rates. The situation became worse owing to the formation and accumulation of blockage

* Corresponding author. Fax: +44 0191 222 5292.
E-mail address: hua.cheng@ncl.ac.uk (H. Cheng).

0378-7753/$ – see front matter © 2013 Elsevier B.V. All rights reserved.
http://dx.doi.org/10.1016/j.jpowsour.2013.02.028

substances (such as CH_3CO_2Li, HCO_2Li and Li_2CO_3) in the cathode, associated with the decomposition of alkyl carbonate electrolytes [7,10–16].

Here we create a three-dimensional nanoporous gas diffusion electrode (GDE) to replace CE as air cathode, which effectively improves battery capacity, rate capability and cycle life. The improvement mechanism is discussed based on electrochemical and spectroscopic characterisations.

2. Experimental

2.1. Synthesis of nanoporous MnO_2 catalyst

Carbon-supported MnO_2 catalyst was synthesised via the following reaction [3,4]:

$$2MnO_4^- + 3Mn^{2+} + 2H_2O \rightarrow 5MnO_2 + 4H^+ \quad (1)$$

2.2. Preparation of gas diffusion electrode and composite electrode

CE was prepared as reported [3,4]; in practice, all of the electrode mixture was spread on a glass plate in one-step, forming an electrode film with a shiny dense structure, as shown later. GDE was fabricated using the same weight ratio as CE (C:MnO_2:-binder:solvent is 10:20:15:45) but with a modified literature methodology [34–36]. The catalyst layer and gas diffusion layer were printed separately. The desired amounts of materials were weighed before making catalyst layer inks, consisting of MnO_2/C, half of Kynar 2801 binder (Elf Atochem), one third of required ether solvent and acetone. They were mixed in an ultrasonic bath for 1 h. A similar procedure was adopted for gas diffusion layer inks with carbon powder (0.5 mg cm^{-2}), half of Kynar binder and one third of required ether solvent plus acetone. A glass microfibre separator (Whatman) was first pre-treated using an electrolyte of 1 M lithium bis-trifluoromethanesulfonyl imide (LiTFSI, 99.95%, Aldrich) in tetraethylene glycol dimethyl ether (TEGDME). Then the catalyst mixture was printed on the rough surface layer of the microfiber layer by layer. Similarly, the mixture for gas diffusion layer was printed layer by layer, covering the catalyst layer. Every layer was dried at 80 °C under Ar atmosphere before spreading a new layer. Finally, a thin layer of mixture of ether and acetone was spread onto the electrode surface. All GDEs were dried overnight at 105 °C under Ar atmosphere. A real mass loading of typical electrodes was 6 mg cm^{-2}.

2.3. Electron microscopy and X-ray diffraction analysis

SEM and TEM images were taken with a JEOL JSM-5300LV scanning electron microscope and a Philips CM100 transmission electron microscope, respectively. XRD analysis was performed with a Siemens D-5005 X-ray Diffractometer. Details for sample preparation and measurement conditions are described in the literature [3,4]. The XRD patterns were compared to the International Centre for Diffraction Data® (ICDD®) [33].

2.4. Electrochemical characterisation

The electrochemical impedance spectra were measured in-situ of batteries, as shown in Fig. 1a, where the cathode was fed with oxygen or argon with a Metrohm Autolab PGSTAT302N Potentiostat/Galvanostat fitted with a frequency response analyser (FRA2 module, Eco Chemie, Holland). The anode served as both reference electrode and counter electrode. The spectra were recorded in a frequency range of 100 kHz to 0.1 Hz with a perturbation amplitude of the ac voltage of 5 mV under open circuit voltage (OCV) conditions [3,4]. The impedance spectra were analysed quantitatively using an equivalent circuit for Li–O_2 batteries [5,11].

To compare gas permeability of MnO_2 GDE and CE materials, the oxygen reduction experiment was carried out in a three-electrode cell with a carbon-supported platinum working electrode (as an oxygen probe), a platinum mesh counter electrode and a Hg_2/Hg_2SO_4 reference electrode, as shown in Fig. 1b. Here the MnO_2

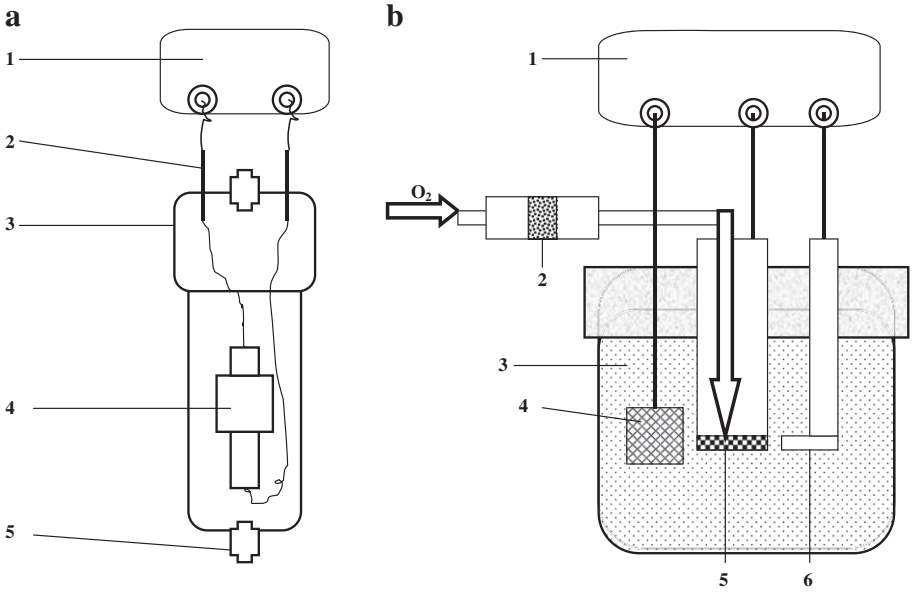

Fig. 1. Schematic diagrams of the electrochemical measurement setups. a. Cycling performance and impedance measurements. 1. Maccor-4200 battery tester or Metrohm Autolab PGSTAT302N Potentiostat/Galvanostats. 2. Current collector. 3. Glass container. 4 The Swagelok cell. 5. Youngs' tap. b. Three-electrode system for measuring gas permeability of MnO_2 gas diffusion electrode and MnO_2 composite electrode materials. 1. Metrohm Autolab PGSTAT302N Potentiostat/Galvanostats. 2. MnO_2 gas diffusion electrode or MnO_2 composite electrode materials (as gas flow barrier). 3. 0.5 M sulphuric acid aqueous solution. 4. Platinum mesh counter electrode. 5. Carbon-supported platinum gas diffusion working electrode (as oxygen probe). 6. Hg/Hg_2SO_4 reference electrode.

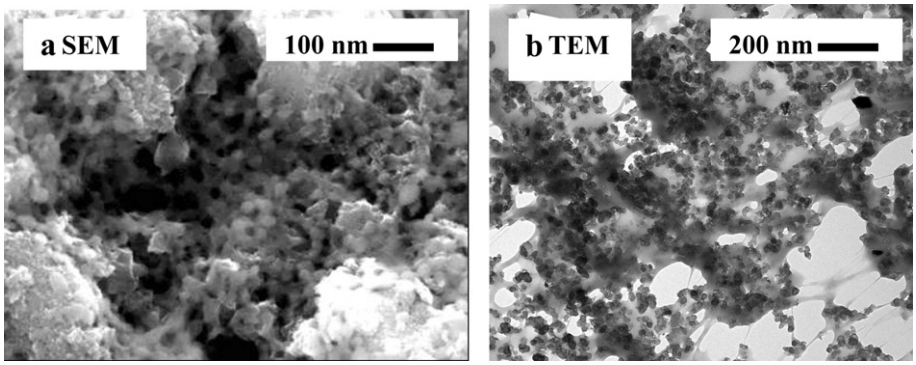

Fig. 2. SEM and TEM images of the nanoporous gas diffusion electrode.

GDE sample was used as a physical barrier for gas flow rather than an oxygen reduction electrode and was compared with the CE sample. Based on the current density produced from oxygen reduction on the carbon-supported Pt probe working electrode when each gas flow barrier was used, we can know how much oxygen passed each flow barrier. The GDE or CE materials, used as gas flow barriers, were placed in a sealed glass tube and oxygen passed through the barrier then come into a PTFE holder which contained the carbon-supported platinum probe working electrode (Fig. 1b). The equipment and procedure for linear sweep voltammetric and potential-step chronoamperometric polarisation measurements was described previously [17–19].

2.5. Batteries and cycle performance test

Fig. 1a shows setup for cycling performance test. The GDE was used as air cathode to assemble a Swagelok type rechargeable Li-air battery with a Li foil anode (Sigma–Aldrich 265985), a glass microfibre filter (Whatman) separator, soaked in 1 M lithium bis-trifluoromethanesulfonyl imide (Aldrich) in tetraethylene glycol dimethyl ether (Aldrich). The Swagelok cells were placed into glass containers (Fig. 1a). Glass containers consist of sealed vacuum tube with two Youngs' taps for gas flow and two electrical pass through connectors (Tempatron Ltd.). The anode and cathode were connected via crocodile clips to the electrical pass through of the encapsulating glass tubes (Fig. 1a). The battery was gastight except for the Al mesh window that exposed the porous cathode to the O_2 atmosphere (1 atm pure oxygen), as shown in Fig. 1a. All processes of assembling and dismantling the batteries were carried out under an argon atmosphere in a glove box (Unilab, MBRAUN, Germany) which provided both water and oxygen levels less than 0.1 ppm. The batteries were first discharged and then charged between 2.0 and 4.0 V (versus Li/Li^+) at different rates (in mA cm^{-2}) using a Maccor-4200 battery test station. Battery tests were performed with a Maccor-4200 battery tester (Maccor) [3,4].

3. Results and discussion

3.1. Comparison of surface morphology

The unique advantage of GDE is its very porous structure, as shown in scanning electron microscopy (SEM) and transmission electron microscopy (TEM) images (Fig. 2). Nanoporous globular or irregular MnO_2 catalyst particles (20–25 nm in diameter, shown as bright spots or agglomerations in Fig. 2a or dark spots in Fig. 2b) are distributed within a porous network of irregular carbon and binder particles (shown as less bright, grey or dark spots or agglomerations in Fig. 2a or bright/grey spots in Fig. 2b). In comparison, a CE shows less porous, denser and more compact network than the GDE with increased degree of agglomeration for MnO_2 particles (Fig. 3a and b). The one-step method to form the CE on a smooth glass plate or the multi-layer method to print the GDE onto the rough fibre could be partly responsible for the difference in surface morphology. The heat treatment of the GDE also played a role in improving porous structure. Consequently, a more porous GDE structure was produced, compared with the conventional CE.

3.2. Comparison of physical and chemical properties

The difference between the GDE and CE in structure directly affected their physical and chemical properties. To assess gas permeability of each material, electrochemical characterisation was carried out in a specially designed three-electrode system, in which a GDE or CE sample was used as a barrier for gas pass. The current

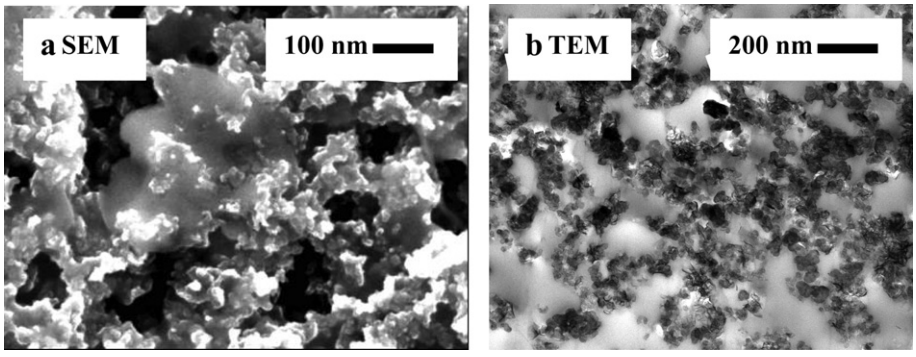

Fig. 3. SEM and TEM images of the composite electrode.

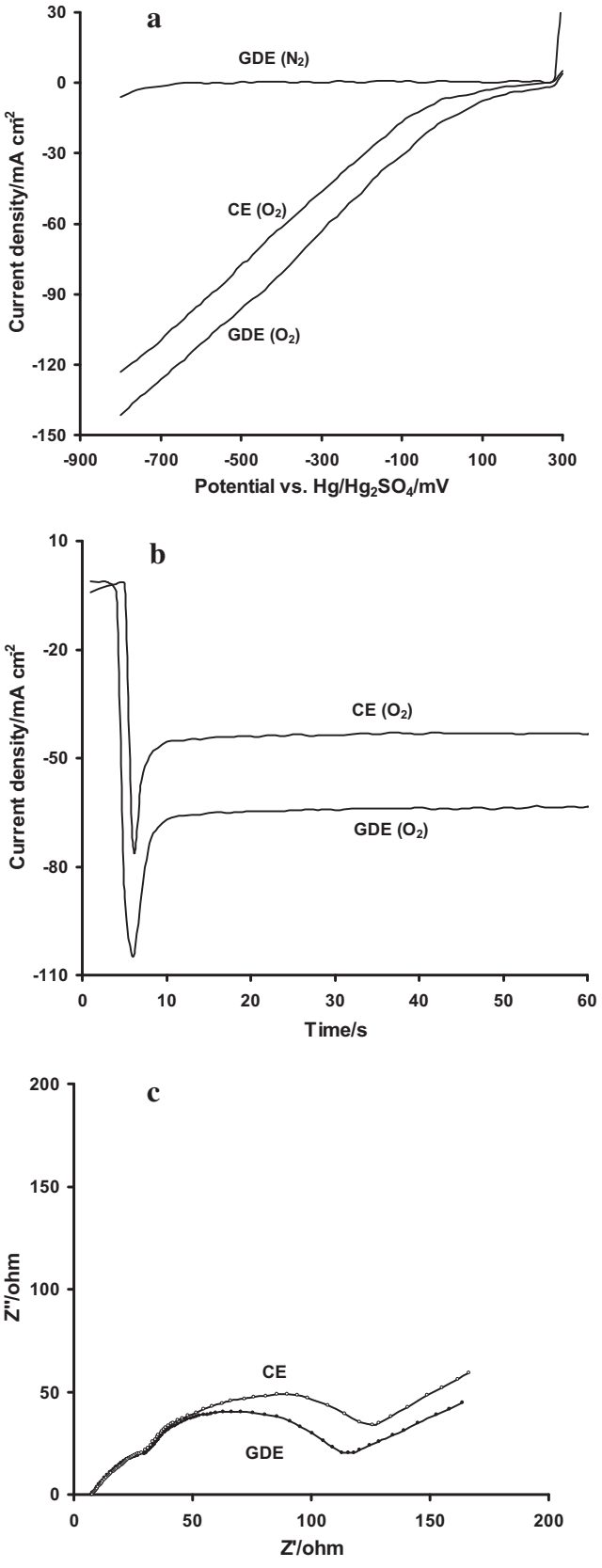

Fig. 4. Electrochemical measurement results of GDE and CE. a. Linear sweep voltammograms (at 30 °C and 1 mV s^{-1}). b. Chronoamperograms (at 30 °C and − 0.2 V vs. Hg/Hg_2SO4). c. Impedance spectra.

produced for oxygen reduction at an oxygen probe was used as a measure of their oxygen permeability, since it is proportional to the amount of oxygen passed through the barrier. Fig. 4a shows their difference, collected via linear sweep voltammetric measurement: 96 versus 75 mA cm^{-2} at − 0.5 V. The feature was confirmed by the steady-state chronoamperometric data (Fig. 4b), suggesting that more oxygen gas passed through the GDE barrier, may be due to more open structure and larger total pore volume than the CE. Superior electronic and ionic transport properties of the nanoporous GDE to CE were demonstrated by the electrochemical impedance spectroscopy (EIS) study. Fig. 4c compares their Nyquist plots. There are the apparent differences in impedance response particularly at medium and low frequencies, implying different charge transfer and mass transport characteristics of both cathodes [5,11,20–26]. This was corroborated by the quantitative analysis of impedance spectra, presented in Table 1: large capacitances and small resistances and impedance, reflecting the high accessible surface area, good conductivity and superb mass transport environment of the GDE [12,13]).

3.3. Battery performance

The GDE was compared with the CE as a cathode in rechargeable Li-air batteries. The GDE battery showed very good capacity-voltage characteristics: provided a 40% increase in initial discharge capacity compared with the CE battery, over 1200 mA h (g solids)$^{-1}$ at a discharge/charge rate of 0.05 mA cm^{-2} (Fig. 5a). Remarkably higher cycle stability was also observed for the GDE battery, compared with its CE counterpart. It is worthwhile to state that there are several units could be chosen to report capacity, including "mA h cm^{-2}", although some units may be more suitable than others in a certain case. We know that "mA h cm^{-2}" may be better when compared to electrode area-related data. In our case, the cathode area was fixed for each battery. Also, the most striking feature of a rechargeable Li-air battery is its high energy density, which is directly related to weight, so "mA h (g solids)$^{-1}$" is a logic choice for us. Here "solids" include all solid components of cathode, i.e. carbon (in both catalyst layer and gas diffusion layer), catalyst and binder etc. Our unit is also different from the currently most popular unit "mA h (g carbon)$^{-1}$", as we believe that all of cathode components contribute to the overall battery weight and, more importantly, the battery capacity is mainly related to the quantity of active materials involved; carbon or catalyst is only one of active components; each component has its irreplaceable role. Therefore, "mA h (g solids)$^{-1}$" may be more reasonable and more accurate than "mA h (g carbon)$^{-1}$". In addition, there is technical convenience to use this unit, which makes data collected from different cathode configurations comparable, particularly when different carbon quantities have to be used, as in this study. Actually, the activity order of cathode materials and conclusions drawing from the capacity data should not be affected by the unit used.

Table 1
Equivalent circuit parameters of rechargeable GDE and CE Li-air batteries.[a]

Cathode	R_{ex}/Ω	R_{in}/Ω	$C_{in} \times 10^6$/F	R_{ct}/Ω	$C_{dl} \times 10^6$/F	W/Ω
GDE (New)	7.5	18.9	4.5	50.7	270.2	0.13
CE (New)	7.8	20.2	3.6	53.5	255.8	0.17
GDE (After 200 cycles)[b]	28.8	48.1	2.8	332.7	216.5	0.24
CE (After 140 cycles)[b]	30.6	56.5	1.3	355.3	185.8	0.35

[a] R_{ex}: external ohmic resistance; R_{in}: interface ohmic resistance; R_{ct}: charge transfer resistance; C_{in}: interface capacitance; C_{dl}: double layer capacitance; W: Warburg impedance.
[b] Data were collected at a discharge/charge rate of 0.05 mA cm^{-2}.

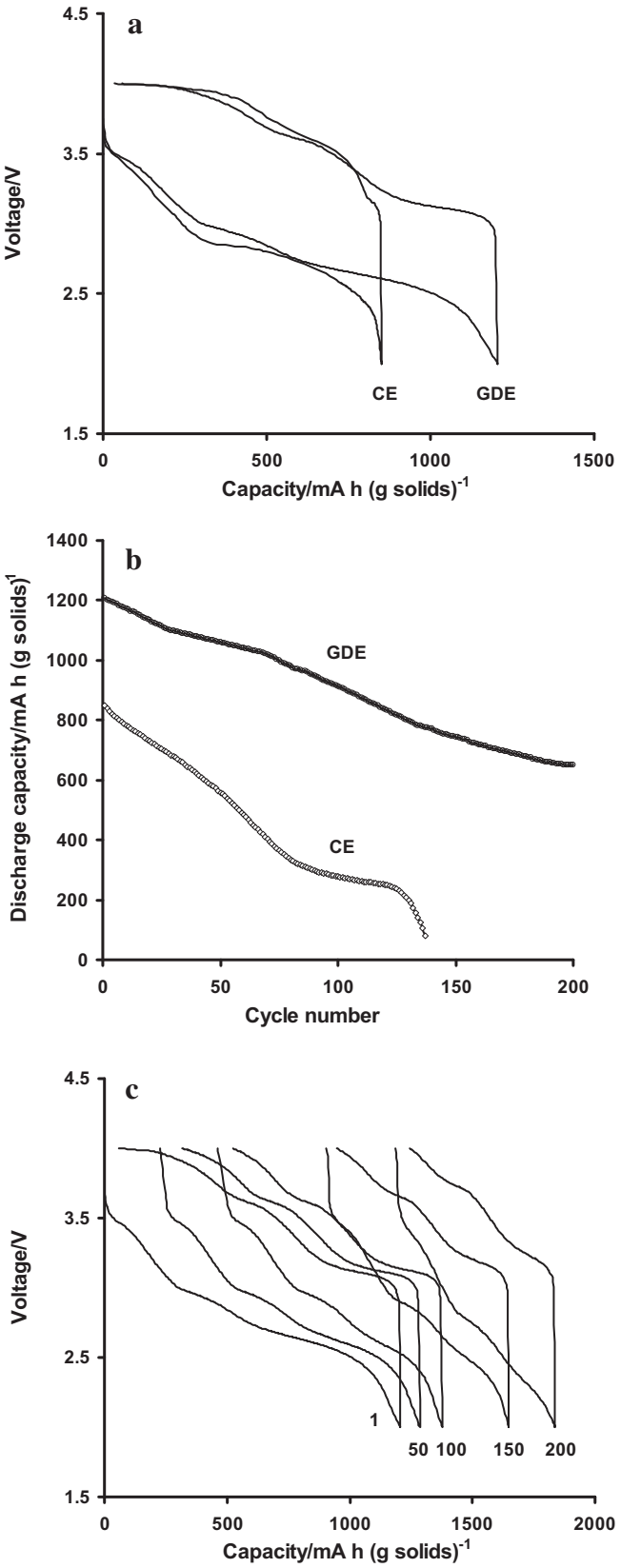

Fig. 5. Charge-discharge characteristics and cycle stability (between 2.0 and 4.0 V at 0.05 mA cm^{-2}, 30 °C) of rechargeable Li-air batteries with GDE and CE. a. Initial charge–discharge curves. b. Cycling performance. c. Charge-discharge curves on cycles 1, 50, 100, 150 and 200.

Table 2
Charge/discharge voltages and discharge capacities of rechargeable GDE and CE Li–O_2 batteries.[a]

Cathode	Voltage[b] (Discharge) (V)	Voltage[b] (Charge) (V)	Capacity[b] (mA h g^{-1})	Capacity retention after cycle			
				50 (%)	100 (%)	140 (%)	200 (%)
GDE	3.0	3.0	1205	88	76	65	54
CE	2.9	3.1	850	65	33	9	

[a] Data were collected at a discharge/charge rate of 0.05 mA cm^{-2}.
[b] Cycle 1.

Fig. 5b compares change tendency of the discharge capacity for two batteries over long-term successive discharge/charge cycles at 0.05 mA cm^{-2}; Fig. 5c shows discharge/charge curves for the GDE battery on cycles 1, 50, 100, 150 and 200. The GDE battery could discharge/charge over 200 cycles whilst the CE battery stopped cycling completely after 140 cycles. This cycle number (200 cycles) is higher than those reported, e.g. 100 cycles at a lower rate of 0.02 mA cm^{-2} with lower storage energy (600–800 mA h (g carbon)$^{-1}$) [27]. The trend could be measured quantitatively by

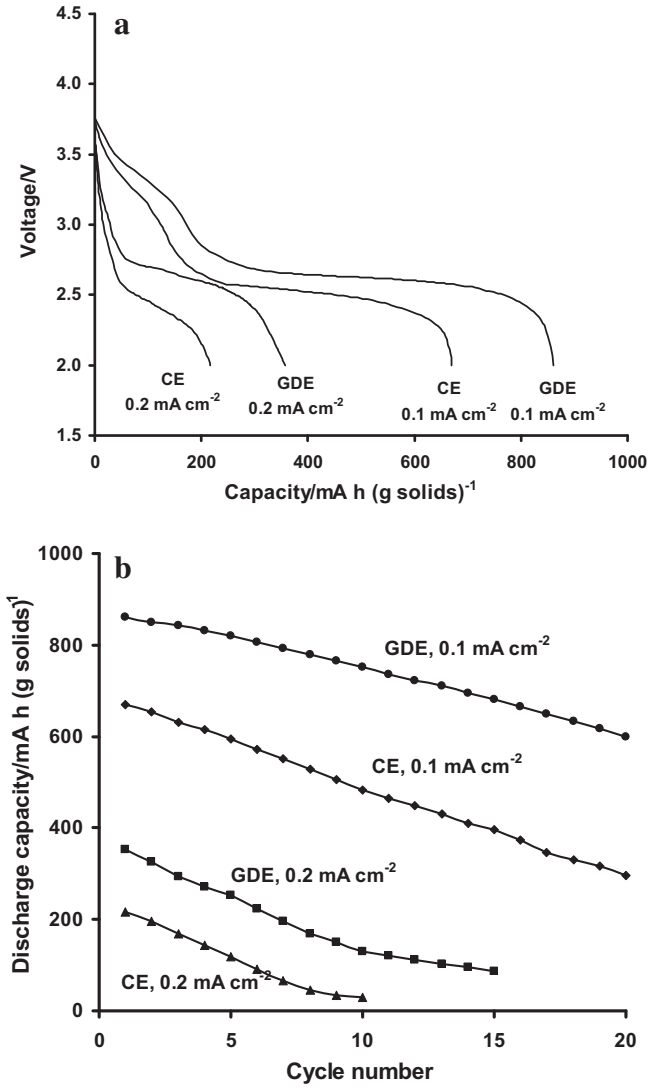

Fig. 6. Cycle stability (between 2.0 and 4.0 V at 0.1 and 0.2 mA cm^{-2}, 30 °C) of rechargeable Li-air batteries with GDE and CE. a. Discharge curves on cycle 1. b. Cycling performance.

capacity retention, defined as the fraction of the full capacity available from a battery under specified conditions of discharge after it has been cycled for a number of cycles. The GDE battery displayed higher capacities at each cycle and higher capacity retention than the CE battery: 88% against 65% and 76% versus 33% after 50 and 100 cycles, respectively. After the CE battery completely failed after 140 cycles with low retention of 9%, the GDE battery could cycle further with retention of 54% after 200 cycles (Table 2). These data clearly demonstrated the advantage of the GDE over the CE in terms of cycling ability.

Superior capacity and cycle ability of the GDE battery to its CE counterpart was also demonstrated at higher discharge/charge rates. The use of GDE rather than CE enhanced charge/discharge rate capability, as corroborated by its higher capacities at all rates (Fig. 6a): 850 vs. 670 mA h (g solids)$^{-1}$) and 360 vs. 220 at 0.1 and 0.2 mA cm^{-2}, respectively. This is also the case for cycling ability, as shown in Fig. 6b: 70% versus 44% retention after 20 cycles at 0.1 mA cm^{-2}. When the discharge/charge rate increased to 0.5 mA cm^{-2}, the CE battery failed after 3 cycles with a low retention of 9.8%, but the GDE battery could cycle further and retained 25% capacity after 10 cycles. At higher rates, e.g. at 1 and 2 mA cm^{-2}, the CE battery could not cycle at all but its GDE counterpart could survive for several cycles. The data highlight the superiority of the GDE over the CE as a cathode material for rechargeable Li-air battery.

3.4. Discussion

The activity of MnO_2 catalyst for oxygen reduction has already been demonstrated for decades in various areas, including in fuel cells and in rechargeable Li-air batteries; this will not be discussed further in this work. As well known, nano-structured gas diffusion electrodes have been widely used in either Zn-air cell or in fuel cell, although we fabricated GDEs using different procedure with different configurations and recipes from those used in Zn-air cell or fuel cell. Also, to our knowledge, application of this type of material in rechargeable Li-air batteries has been rarely reported and we had some new discoveries about its application. In fact, our GDE is different from the composite electrode, from fabrication procedure to properties, such as: (i) The CE is a shiny film with less porosity than the GDE that was not shiny with a rough surface. (ii) SEM and TEM also proved that the CE is denser with less porosity than the GDE. (iii) The gas flow barrier experiment proved that less oxygen passed through the CE barrier material and, therefore, smaller current from the oxygen reduction was detected at the carbon-supported Pt probe electrode, compared with the GDE. (iv) The cycling performance also confirmed their differences. The mechanism for the greater improvement of the GDE than CE could be drawn from electrochemical and spectroscopic evidences, mainly in the following aspects:

(i) Surface morphology. As mentioned early, the new GDE had more porous structure than the new CE. This remains the case at all stages of cycling; after cycling, the GDE cathode exhibited less degree of agglomeration and better retained porous structure (Fig. 7a and b) as well as more small catalyst particles and clusters/blocks (Fig. 7c and d) even experienced 60 more cycles. This not only indicates higher porosity and more interconnected channels for the electrolyte and oxygen but also implies more electrochemical active sites on the GDE than CE [28,29].
(ii) Active materials. The SEM and TEM images had already displayed greater dispersion and less agglomeration of catalyst, suggesting lower polarisation of the GDE than CE [28,30,31].

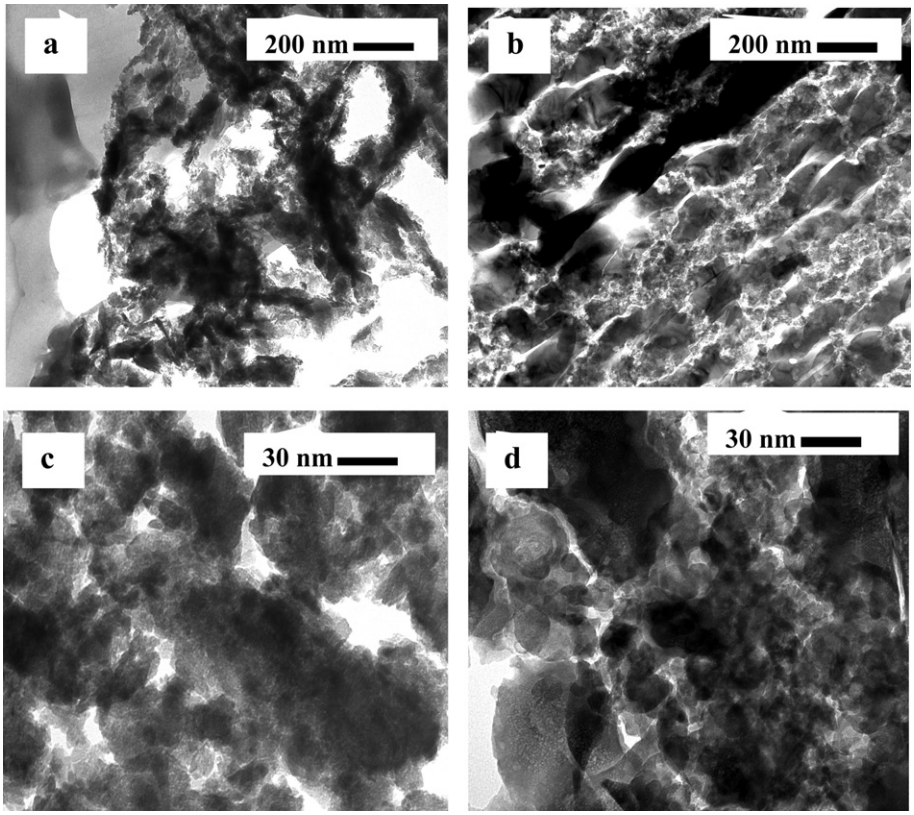

Fig. 7. TEM images of the nanoporous gas diffusion electrode and composite electrode after cycling between 2.0 and 4.0 V at 0.05 mA cm^{-2} and 30 °C A and c. GDE, after 200 cycles. b and d. CE, after 140 cycles.

Also, the XRD measurement proved less catalyst loss in the GDE than CE, as evidenced by smaller reduction in main peak intensities (MnO_2 (100), MnO_2 (101), MnO_2 (102) and MnO_2 (110) for ε-MnO_2 catalyst [32,33]) (Fig. 8a). This means that the GDE was more capable to hold the MnO_2 catalyst than the CE, providing higher activity/capacity and capacity retention at all stages of cycling. The GDE had exhibited less loss of electrolyte than the CE, which was indirectly demonstrated by measuring battery conductivity of each battery via impedance measurements, as shown in Fig. 8b and Table 1: the external resistance increased more than 36 Ω for the CE but only 29 Ω for the GDE. The less loss of electrolyte of the GDE provided more benign existing media for transport of Li ion, intermediates and products as well as less over flooding the electrode [34] than CE. Fig. 8a also shows less Li_2CO_3 formation in the GDE than the CE, indirectly indicating less electrolyte decomposition and lower degree of side reactions of the former [10]. Since insoluble Li_2CO_3 solid constituted physical barriers for mass transfer of all species involved, so the GDE allowed a better transfer of all species than the CE at all cycling stages, leading to larger capacity, higher rate capability and higher cycle stability. There were several factors affecting the formation and accumulation of Li_2CO_3. For example, more holes could be left on the CE owing to its greater loss of MnO_2 than the GDE in terms of catalyst itself. But this could not totally compensate its less porous structure arising from its original dense structure, hence, this factor could be ruled out. As well known, during the cycling process, highly reactive oxygen radicals could lead to the formation of lithium peroxides/oxides, as well as attacked electrolyte to form Li_2CO_3 [10]. Quite possibly, there were different degrees of the competition between the main reaction and the formation of Li_2CO_3 on the GDE and CE, which were in favouring less formation of Li_2CO_3 at the GDE for some reasons (e.g. oxygen reactions went through more quickly). Another possible source may be their varying degrees of mass transport because of their different porous structure and less pore clogging of the GDE. As for different catalyst losses, this may be due to their difference in brittleness; the CE was generally more brittle and was lost more than the GDE, as could be seen from comparison both types of electrodes after cycling. Also, it could be due to different degrees of agglomeration; the loss of larger catalyst agglomerates in the CE may lead to its greater percentages of catalyst loss, compared with the GDE. More resilient structure of the GDE may play a role in maintaining catalyst. In order to understanding the observation thoroughly, further investigation is required.

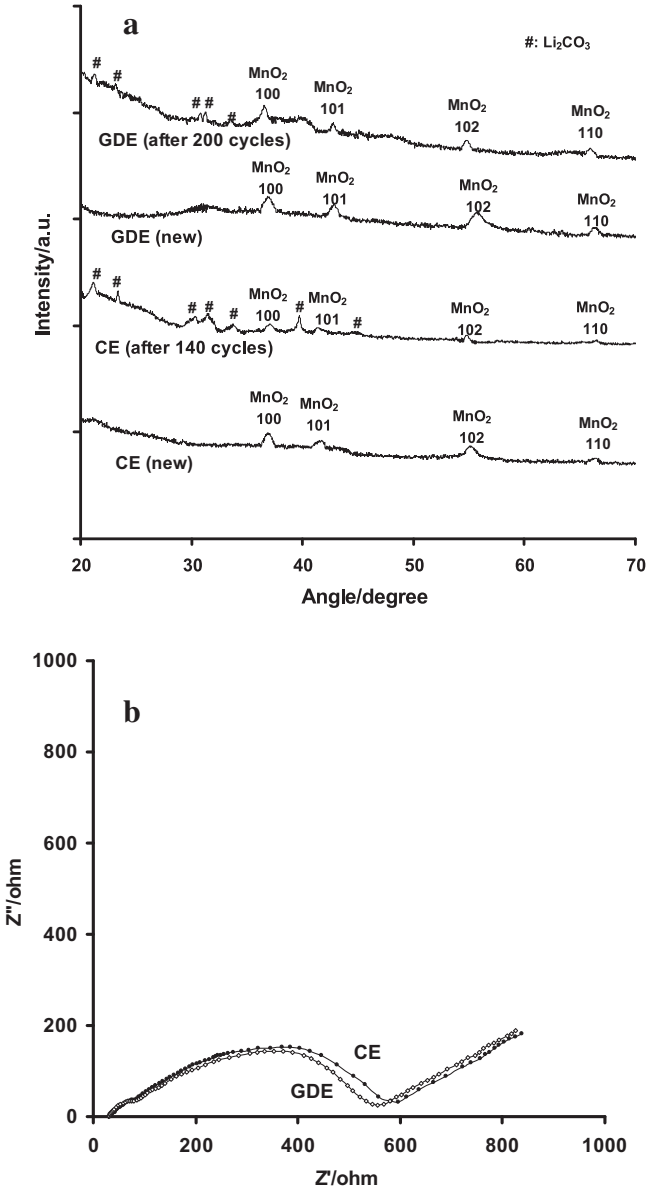

Fig. 8. X-ray powder diffraction patterns (a) and impedance spectra (b) of GDE (after 200 cycles) and CE (after 140 cycles) between 2.0 and 4.0 V at 0.05 mA cm^{-2} and 30 °C.

(iii) Electrochemical properties. The new GDE exhibited lower resistance/impedance and higher capacitance than the CE (Fig. 4c, Table 1). The trend remained after cycling; as shown in Fig. 8b and Tale 1: the Warburg resistance (diffusion impedance) increased from 0.17 to 0.35 Ω for the CE but only 0.13 to 0.24 Ω for the GDE and the capacitance reduced to 70 and 54 mF for the CE and GDE, respectively. These data reflected a less change in the porosity and less build up of discharge products within the pores, a better ionic diffusion, larger accessible electrode surface area and more efficient reaction within the GDE than CE [5,14,15,35,36].

4. Conclusions

In summary, we have validated the good fit of nano-structured three-dimensional GDE for a rechargeable Li-air battery and its ability to replace the CE, giving promise long-term stability with superb capacity and discharge/charge rate. The improvement mechanism of the GDE was proposed based on charge/discharge curves, electrochemical and spectroscopic evidences. The superior nano-structure of the GDE to CE played a key role, promoting formation of more effective three phase region, acting as an interconnected micro-network with electrolyte-filled pore and shorter diffusion distances for lithium ions and electrons as well as better accommodation environment for gas and liquid reactants and products. In addition, less loss of catalyst and electrolyte, more available active sites and higher surface area in contact with electrolyte of the GDE than CE facilitated its more effective oxygen reduction reaction, reduced formation of Li_2CO_3 and other blockage substances and provided superior electrochemical properties. All of these factors made the GDE a better cathode material than the CE, delivering higher capacities and larger discharge/charge rates and maintaining its advantages at all cycling stages, thus showed higher cycle stability. Considering the fact that the instability sources of our batteries were not completely removed, with further optimisation of the GDE plus other new materials (such as more stable and Li-compatible electrolyte), much higher capacity, rate capability

and cycling stability are likely. The issue will be the focus of our future studies.

Acknowledgements

The authors thank the EPSRC for funding. TEM measurements provided by the Electron Microscopy Research Services at Newcastle University. SEM, EDX and XRD measurements provided by the Advanced Chemical & Materials Analysis Services at Newcastle University.

References

[1] D. Graham-Rowe, New Scientist 18 (2012) 2846.
[2] G. Girishkumar, B. McCloskey, A.C. Luntz, S. Swanson, W. Wilcke, J. Phys. Chem. Lett. 1 (2010) 2193.
[3] H. Cheng, K. Scott, Appl. Catal. B: Environ. 108–109 (2011) 140.
[4] H. Cheng, K. Scott, J. Power Sources 195 (2010) 1370.
[5] M. Mirzaeian, P.J. Hall, J. Power Sources 195 (2010) 6817.
[6] A. Debart, J.L. Bao, G. Armstrong, P.G. Bruce, J. Power Sources 174 (2007) 1177.
[7] T. Ogasawara, A. Debart, M. Holzapfel, P. Novak, P.G. Bruce, J. Am. Chem. Soc. 128 (2006) 1390.
[8] W. Xu, J. Xiao, D. Wang, J. Zhang, J.-G. Zhang, J. Electrochem. Soc. 157 (2010) A219.
[9] W. Xu, J. Xiao, D. Wang, J. Zhang, J.-G. Zhang, Electrochem. Solid-state Lett. 13 (2010) A48.
[10] S.A. Freunberger, Y. Chen, Z. Peng, J.M. Griffin, L.J. Hardwick, F. Bardé, P. Novák, P.G. Bruce, J. Am. Chem. Soc. 133 (2011) 8040.
[11] X. Yang, Y. Xia, J. Solid State Electrochem. 14 (2010) 109.
[12] C.Y. heng, G. Wang, M. Yan, Z. Jiang, J. Solid State Electrochem 11 (2007) 310.
[13] P.B. Balbuena, Y. Wang, Lithium-ion Batteries: Solid-electrolyte Interphase, Imperial College Press, London, 2004, Ch. 1.
[14] T. Kawamura, S. Okada, J. Yamaki, J. Power Sources 156 (2006) 547.
[15] A.V. Plakhotnyk, L. Ernst, R. Schmutzler, J. Fluorine Chem. 126 (2005) 27.
[16] J.S. Gnanaraj, V.G. Pol, A. Gedanken, D. Aurbach, Electrochem. Commun. 5 (2003) 940.
[17] H. Cheng, W. Yuan, K. Scott, J. Power Sources 183 (2008) 678.
[18] H. Cheng, W. Yuan, K. Scott, D.J. Browning, J.B. Lakeman, Appl. Catal. B: Environ. 75 (2007) 221.
[19] H. Cheng, W. Yuan, K. Scott, D.J. Browning, J.B. Lakeman, J. Power Sources 172 (2007) 597.
[20] F. Croce, F. Nobili, A. Deptula, W. Lada, R. Tossici, A.D. Epifanio, B. Scrosati, R. Marassi, Electrochem. Commun. 1 (1999) 605.
[21] R. Fong, R. Von Sacken, U.J. Dahn, J. Electrochem. Soc. 137 (1990) 2009.
[22] N. Takami, A. Satoh, M. Hara, T. Ohsaki, J. Electrochem. Soc. 142 (1995) 371.
[23] S. Passerini, J.M. Rosolen, B. Scrosati, J. Power Sources 45 (1993) 333.
[24] J. Thevenin, R.H. Muller, J. Electrochem. Soc. 134 (1987) 237.
[25] J.Y. Song, H.H. Lee, Y.Y. Wang, C.C. Wan, J. Power Sources 111 (2002) 255.
[26] J. Fan, P.S. Fedkiw, J. Power Sources 72 (1998) 165.
[27] F. Mizuno, S. Nakanishi, Y. Kotani, S. Yokoishi, H. Iba, Electrochemistry 78 (2010) 403.
[28] Y. Lin, X. Cui, X. Ye, Electrochem. Commun. 7 (2005) 267.
[29] L. Zhang, K. Lee, J. Zhang, Electrochim. Acta 52 (2007) 7964.
[30] K. Ding, G. Yang, S. Wei, P. Mavinakuli, Z. Guo, Ind. Eng. Chem. Res. 49 (2010) 11415.
[31] R. Pattabiraman, Appl. Catal. A – Gen. 153 (1997) 9.
[32] The International Centre for Diffraction Data®, http://www.icdd.com/(the reference codes are 00-030-0820 for MnO_2, 009-0355 for Li_2O_2, 012-0254 for Li_2O and 00-022-1141 for Li_2CO_3).
[33] A.J. Roberts, R.C.T. Slade, J. Mater. Chem. 20 (2010) 3221.
[34] C. Tran, X. Yang, D. Qu, J. Power Sources 195 (2010) 2057.
[35] H. Arai, S. Muller, O. Haas, J. Electrochem. Soc. 147 (2000) 3584.
[36] N. Jia, R.B. Martin, Z. Qi, M.C. Lefebvre, P.G. Pickup, Electrochim. Acta 46 (2001) 2863.